35th Annual International Conference of the IEEE EMBS
Osaka, Japan, 3 - 7 July, 2013

Cell-specific Modeling of Retinal Ganglion Cell Electrical Activity

Tianruo Guo, *Student Member, IEEE,* David Tsai, *Member, IEEE,* John W. Morley, Gregg J. Suaning, *Senior Member, IEEE*, Nigel H. Lovell, *Fellow, IEEE* and Socrates Dokos, *Member, IEEE*

***Abstract*—Variations in ionic channel expression and anatomical properties can influence how different retinal ganglion cell (RGC) types process synaptic information. Computational modeling approaches allow us to precisely control these biophysical and physical properties and isolate their effects in shaping RGC firing patterns. In this study, three models based on realistic representations of RGC morphologies were used to simulate the contribution of spatial structure of neurons and membrane ion channel properties to RGC electrical activity. In all simulations, the RGC models shared common ionic channel kinetics, differing only in their regional ionic channel distributions and cell morphology.**

I. Introduction

It is commonly accepted that around 20 distinct retinal ganglion cell (RGC) types are present in the mammalian retina [1, 2]. Each RGC type transfers specific visual information from photoreceptor cells to higher visual centers in the brain via their axons, due to their unique intrinsic biophysical and anatomical properties, as well as integration of their synaptic inputs. Over the past several decades, computational models have become increasingly important for understanding the underlying ionic mechanisms in RGC electrophysiology [3-5]. However, apart from a recent study in our laboratory [6], prior models of RGCs have been largely limited to the single-compartment level or identification of individual RGC types without regard to the functional significance of cellular morphology and membrane channel distributions in each cellular region, despite the correlation between their function and inherent biophysical/physical properties suggested by experimental studies [1, 7].

Moreover, no studies have attempted to simulate the mechanisms underlying rebound excitation with complete anatomical reconstruction of functionally-identified RGCs. Rebound activity (also termed post-inhibitory rebound) is defined by a period of increased excitability following termination of a hyperpolarizing stimulus. This mechanism can convert inhibitory signals into an excitatory signal. It has been studied in a number of neuronal types and contributes to neuronal information processing under many physiological and pathological conditions [8]. In particular, rebound activity in the retina has been hypothesized to play an important role in visual information encoding [9].

In this study, we have used a realistic modeling approach to study the biophysical/physical mechanisms underlying multiple functionally-identified RGC types. Existing ionic models were modified by adding ionic currents known to respond to hyperpolarizing stimuli. With optimized cell-specific model parameters and the incorporation of detailed cell morphologies, our models were able to closely reproduce RGC responses in various cells.

T. Guo, D. Tsai, G. J. Suaning, N. H. Lovell and S. Dokos are with the Graduate School of Biomedical Engineering, University of New South Wales, Sydney, 2052, Australia. D. Tsai is also with the Howard Hughes Medical Institute, Biological Sciences, Columbia University, New York, NY, USA and Bioelectronic Systems Lab, Electrical Engineering, Columbia University, New York, NY, USA. J. W. Morley is with School of Medicine, University of Western Sydney, Australia.

E-mail for correspondence: t.guo@unsw.edu.au

II. Methodology

A. Morphologically-realistic RGC models

The RGC model used in this study can be represented by the equivalent cable equation:

$$\sigma \frac{\partial^2 V_m}{\partial x^2} = A(C_m \frac{dV_m}{dt} + J_{ion} - J_{stim}) \quad (1)$$

where V_m represents membrane potential, x is the axial cable distance, σ is the intracellular conductivity ($mS \cdot cm^{-1}$), A is the local cell surface to volume ratio (cm^{-1}), and membrane capacitance (C_m) per unit membrane area was set to 1 $\mu F \cdot cm^{-2}$. The intracellular axial resistivity ($1/\sigma$) was set to 110 Ω·cm. J_{stim} represents the intracellular stimulus. The simulation temperature was 35 °C. J_{ion} ($\mu A \cdot cm^{-2}$) represents the ionic currents, which consist of seven time-dependent currents and one leakage current:

$$J_{ion} = I_{Na} + I_K + I_{KA} + I_{Ca} + I_{KCa} + I_h + I_{CaT} + I_L \quad (2)$$

where most of these (except for two as described below) are defined in the Fohlmeister and Miller (FM) RGC model [10]. We also added a hyperpolarization-activated current (I_h) and a low-threshold voltage-activated calcium current (I_{CaT}), which are both known to contribute to neuronal excitation following hyperpolarization [11]. I_h and I_{CaT} were described by standard Hodgkin-Huxley-type [12] formulations:

$$I_h = \bar{g}_h \, y \, (V_m - V_h) \quad (3)$$

$$I_{CaT} = \bar{g}_{CaT} \, m^3 \, h \, (V_m - V_{CaT}) \quad (4)$$

where $\bar{g}_h$ and $\bar{g}_{CaT}$ are the maximum membrane conductances. The reversal potentials (V_h and V_L) for I_h and I_L were -26.8 and -75 mV, respectively. V_{CaT} was formulated as a function of cytosolic calcium concentration, according to the Nernst equation [10]. The gating kinetics of I_h and I_{CaT} were governed by:

$$I_h: \frac{dy}{dt} = \frac{y_\infty - y}{\tau_h},\ y_\infty = \frac{1}{1+e^{(V+75)/5.5}},\ \tau_h = \frac{588.2 \cdot e^{0.01(V+20)}}{1+e^{0.2(V+20)}} \quad (5)$$

$$I_{CaT}: \frac{dm}{dt} = \alpha_m(1-m) - \beta_m m,\ \frac{dh}{dt} = \alpha_h(1-h) - \beta_h h,$$

$$\alpha_m = \frac{0.91}{1+e^{-0.17(V+61.5)}},\ \beta_m = \frac{0.64}{1+e^{-0.03(V+10)}} + \frac{0.64}{1+e^{0.2(V+89.4)}}$$

$$\alpha_h = 0.013e^{0.022(V+131.1)},\ \beta_h = \frac{0.9}{1+e^{-0.02(V+42.9)}} \quad (6)$$

TABLE I.
IONIC CHANNEL DISTRIBUTIONS

Channel	Regional Maximum Membrane Conductances (mS/cm^2)				
	Soma	**Axon**	**AIS**	**Hillock**	**Dendrites**
ON					
I_{Na}	51	51	510	51	19.1
I_K	13.1	13.1	13.1	13.1	8.73
I_{KA}	39.4	-	39.4	39.4	26.27
I_{Ca}	1.1	-	1.1	1.1	1.47
I_{KCa}	0.047	0.047	0.047	0.047	7.23e-4
I_h	0.11	0.11	0.11	0.11	0.11
I_{CaT}	0.029	0.029	0.029	0.029	0.145
I_L	0.147	0.147	0.147	0.147	0.147
OFF					
I_{Na}	45.9	45.9	459	45.9	17.2
I_K	13.1	13.1	13.1	13.1	8.73
I_{KA}	39.4	-	39.4	39.4	26.27
I_{Ca}	1.1	-	1.1	1.1	1.47
I_{KCa}	0.47	0.47	0.47	0.47	7.23e-4
I_h	0.383	0.383	0.383	0.383	0.383
I_{CaT}	0.052	0.052	0.052	0.052	0.26
I_L	0.147	0.147	0.147	0.147	0.147
OFF P					
I_{Na}	48	48	480	48	18
I_K	25.2	25.2	25.2	25.2	16.8
I_{KA}	18.9	-	18.9	18.9	12.6
I_{Ca}	2.2	-	2.2	2.2	2.94
I_{KCa}	0.047	0.047	0.047	0.047	7.23e-4
I_h	0.132	0.132	0.132	0.132	0.132
I_{CaT}	0.017	0.017	0.017	0.017	0.085
I_L	0.07	0.07	0.07	0.07	0.07

Cell morphologies were identified by their dendritic field size/structure, and stratification in the inner plexiform layer (IPL). An ON cell with 196 µm average dendritic diameter and stratified at a depth of ~40% in the IPL (the edge of ganglion cell layer being 0%), an OFF cell (191 µm average dendritic diameter, at a depth of ~70% in the IPL) and an OFF parasol cell (208 µm average dendritic diameter, at a depth of ~90% in the IPL) were traced from mice retinae. Morphological data were digitized and subsequently imported into the NEURON computational software [13], which approximated the cable equation (1) into a multi-compartmental representation of the neuron, equivalent to a finite-difference approximation of the spatial second derivative. Details of procedures for RGC morphological reconstruction are described in [14].

B. Current-clamp recording

Mice RGCs were targeted for recording in the inferior retina. Somatic whole-cell current clamp recordings were made using glass electrodes with resistances of 3.0 ~ 5.0 MΩ. Series resistance was compensated accordingly on the amplifier (MultiClamp 700B, Molecular Devices). Data were low-pass filtered at 10 kHz and digitized at 50 kHz on a computer running pClamp 10 (Molecular Devices). All data were analyzed in pClamp 10 and Matlab R2010a (Mathworks). In order to isolate the contribution of biophysical properties and morphologies, all RGC excitatory and inhibitory synaptic inputs were pharmacologically blocked during recording. All procedures were approved and monitored by the University of New South Wales Animal Care and Ethics Committee.

C. Parameter optimization using shared and cell-specific parameters

The RGC models were simultaneously fitted to three action potential (AP) datasets recorded from ON, OFF and OFF Parasol cells shared kinetic and cell-specific maximum membrane conductance ($\bar{g}_j$) parameters (an indicator of ion channel density). Each group included RGC voltage responses recorded during depolarizing and hyperpolarizing somatic current injections (500 ms duration, -210 ~ 120 pA, in 30 pA steps). Parameter values were optimized by minimizing the sum of squares of the difference between the experimental data and the corresponding model outputs, using a custom curvilinear, gradient-based optimization method [15]. We assumed that firing pattern variations were due to the differential distribution of ion channels and cell morphologies among the three RGC types.

III. RESULTS

A. Cell-specific responses

The ionic channel distributions were compartment-specific to reflect the proportion of ion channels in specific regions of each RGC. The optimized maximum membrane conductance values per region in each cell are listed in Table I. Three RGC models exhibited significantly different channel densities (Fig. 1A) and morphologies (Fig. 1B), which contributed to the cell-specific AP firing patterns in response to multiple somatic injections. OFF and OFF Parasol cells demonstrated marked excitation in response to hyperpolarizing stimuli, including a time-dependent depolarizing "sag" (~17 and ~11 mV respectively) during hyperpolarization below the resting membrane potential. They also exhibited different levels of rebound spike rate following the termination of hyperpolarizing stimulus. The ON cell only showed a relatively small sag (~3 mV), despite having a much higher

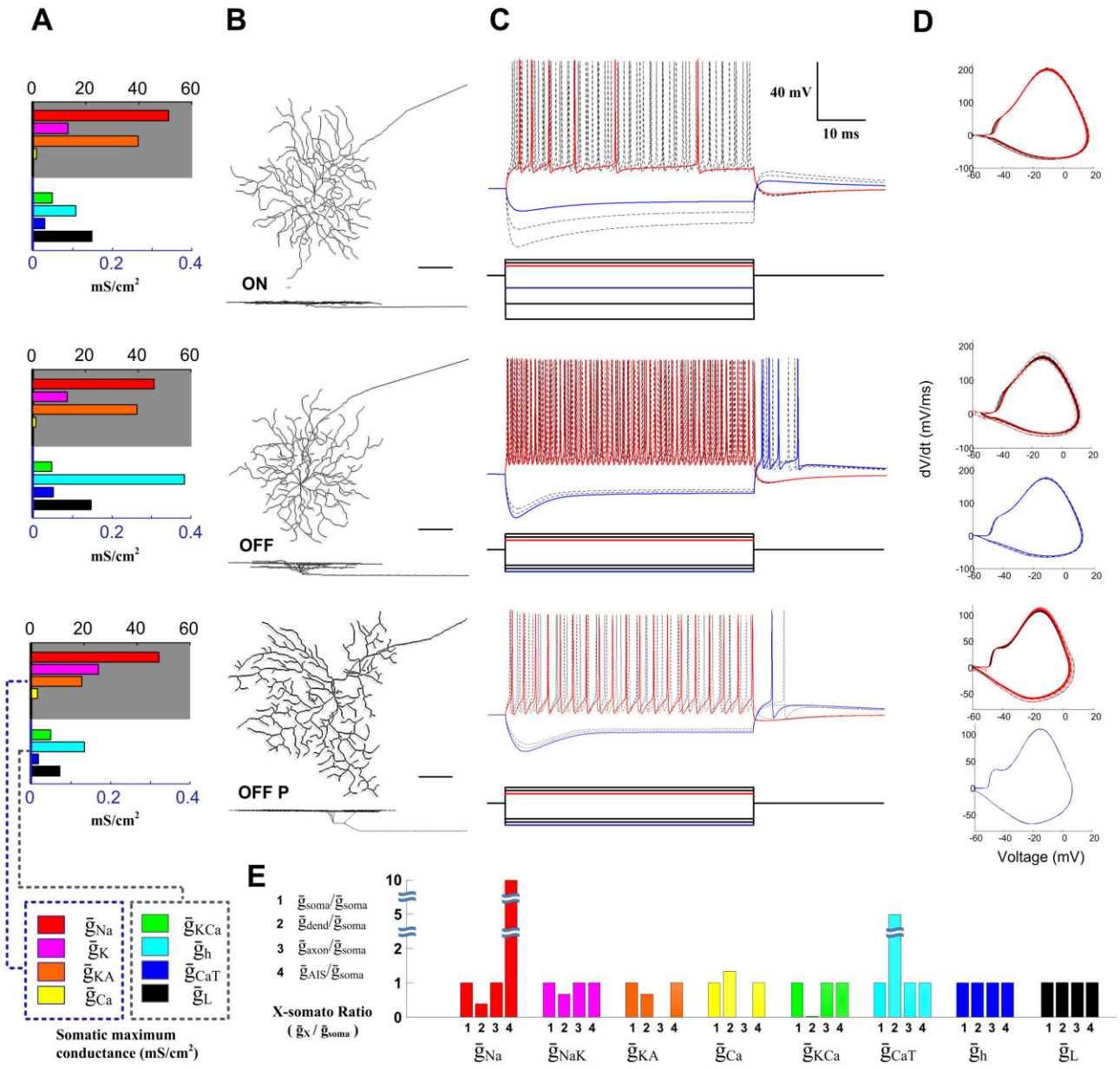

Fig. 1 Distinct firing patterns reproduced by the RGC models. A. Somatic channel maximum membrane conductance in each RGC. Note the different current scales for high (black) and low (red) densities. B. Mice RGC morphologies for ON, OFF, and OFF parasol cells. Scale bar: 40 µm. C. Membrane potentials in response to multiple depolarizing (red) and hyperpolarizing (blue) somatic current injections in each RGC. Resting potentials were -62, -65 and -60 mV respectively. External somatic current injection: 500 ms duration with amplitudes of 100, 120 and 140 pA for depolarizing injection for all cells, 120, 140 and 160 pA for hyperpolarizing injection for OFF and OFF Parasol cells and 120, 200, 300 pA for the ON cell. Red and blue traces highlight individual depolarized and hyperpolarized responses corresponding to the step commands (of the same colour) below. Scale bar: 40 mV and 10 ms. D. Phase plot (dV/dt versus V) of the somatic depolarizing (red) and rebound (blue) AP in each RGC. Note the absence of rebound spiking in the ON cell. E. Ionic channel distribution ratio between each RGC region and the soma (defined as $\bar{g}_{j,\,x}/\bar{g}_{j,\,soma}$).

hyperpolarizing amplitude (300 pA compared with 160 pA in the OFF cells). Furthermore, these three cell types exhibited different spiking frequency and latency in response to the same levels of stimuli (highlighted in the red and blue traces of Fig. 1C). The rate of membrane voltage change (Fig. 1D) differed between each cell type. All of these responses closely matched the experimental recordings from each RGC. Fig. 2 shows fitted APs for an OFF Parasol cell following multi-dataset based optimization. The model can reproduce realistic firing properties polarized in either direction of the resting membrane potential (500 ms duration, with stimulus amplitudes of -120, -90, -60, 0, 60, 90, 120, and 150 pA), including the patterns of depolarizing sag, frequency adaptation, firing latency, as well as the firing property variations caused by different stimulus amplitudes.

IV. Discussion and Conclusion

In this study, a significant improvement over existing modeling approaches [3, 4, 6] was that we could generate biological responses in different functionally-identified RGCs using cell-specific ion channel properties and morphologies. Our technique provides a promising platform to establish a basis for realistic modeling of cellular electrical activity in the entire RGC population.

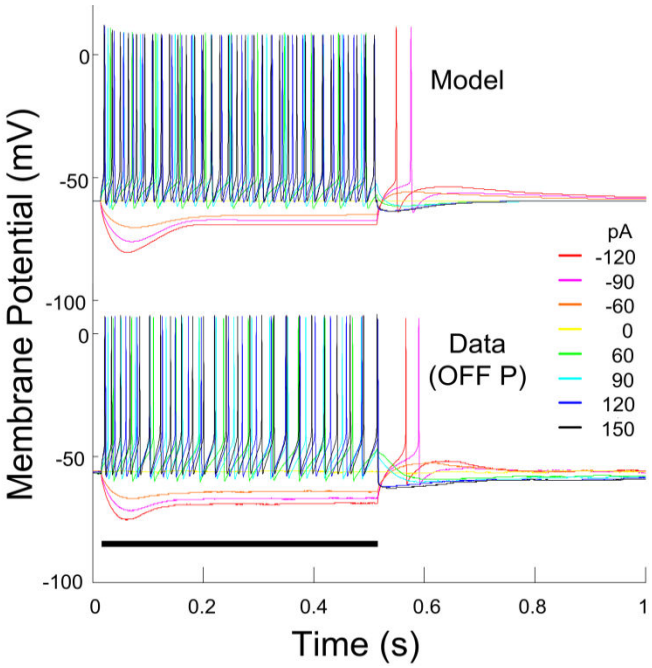

Fig. 2. Comparison of OFF Parasol RGC model to experimental APs in response to multiple somatic injections. Upper: Multiple model-generated membrane potentials in response to a family of somatic current pulses. Colored traces correspond to each pulse amplitude in the legend. Lower: Experimental AP responses obtained in OFF parasol RGC while injecting the same level of somatic current via a patch electrode. Horizontal bar: stimulus duration.

Compared to previous RGC models, our model included higher I_{Na} in the axonal initial segment (AIS) (tenfold to somatic density versus ~twofold in the FM model). For the new currents, we set a high dendritic I_{CaT} density (sixfold to that in soma) as suggested by the experimental evidence [16]. Differences in ionic channel distributions between RGC types raise the possibility that each type may exhibit markedly different firing patterns in response to the identical inputs. For example, the rebound excitation recorded in OFF and OFF Parasol cells could be due to their higher I_h and I_{CaT} densities compared to that of the ON cells. Moreover, an identical depolarizing stimulus strongly activated OFF cells; only weakly excited OFF Parasol cells and minimally activated the ON cells (see Fig.1C). These results reveal a large range of threshold variations among different RGC types. Neuronal morphologies can influence the flow of intracellular currents between neighboring compartments by their specific cell membrane area and intracellular resistivity. As a result, this could also contribute to the unique behaviors of different RGC types. The critical roles of RGC morphologies in shaping their firing patterns are discussed in an accompanying paper [14]. In future studies, we intend to expand analysis to additional RGC types in order to build comprehensive models of the electrical responses of the various RGCs which contribute to our perception of vision.

Acknowledgment

This research was supported by the Australian Research Council (ARC) through a Special Research Initiative in Bionic Vision Science and Technology grant to Bionic Vision Australia. We thank Dr Amr Al Abed for his critical comments.

References

[1] B. J. O'Brien, T. Isayama, R. Richardson, and D. M. Berson, "Intrinsic physiological properties of cat retinal ganglion cells," *J Physiol,* vol. 538, pp. 787-802, 2002.

[2] B. Volgyi, S. Chheda, and S. A. Bloomfield, "Tracer coupling patterns of the ganglion cell subtypes in the mouse retina," *J Comp Neurol,* vol. 512, pp. 664-687, 2009.

[3] J. F. Fohlmeister, E. D. Cohen, and E. A. Newman, "Mechanisms and distribution of ion channels in retinal ganglion cells: using temperature as an independent variable," *J Neurophysiol,* vol. 103, pp. 1357-1374, 2010.

[4] T. Kameneva, H. Meffin, and A. N. Burkitt, "Modelling intrinsic electrophysiological properties of ON and OFF retinal ganglion cells," *J Comput Neurosci,* vol. 31, pp. 547-561, 2011.

[5] M. J. Schachter, N. Oesch, R. G. Smith, and W. R. Taylor, "Dendritic spikes amplify the synaptic signal to enhance detection of motion in a simulation of the direction-selective ganglion cell," *Plos Comput Biol,* vol. 6, 2010.

[6] D. Tsai, S. Chen, D. A. Protti, J. W. Morley, G. J. Suaning, and N. H. Lovell, "Responses of retinal ganglion cells to extracellular electrical stimulation, from single cell to population: model-based analysis," *PLoS One,* vol. 7, p. e53357, 2012.

[7] R. C. Wong, S. L. Cloherty, M. R. Ibbotson, and B. J. O'Brien, "Intrinsic physiological properties of rat retinal ganglion cells with a comparative analysis," *J Neurophysiol,* vol. 108, pp. 2008-2023, 2012.

[8] R. Boehme, V. N. Uebele, J. J. Renger, and C. Pedroarena, "Rebound excitation triggered by synaptic inhibition in cerebellar nuclear neurons is suppressed by selective T-type calcium channel block," *J Neurophysiol,* vol. 106, pp. 2653-2661, 2011.

[9] D. J. Margolis and P. B. Detwiler, "Different mechanisms generate maintained activity in ON and OFF retinal ganglion cells," *J Neurosci,* vol. 27, pp. 5994-6005, 2007.

[10] J. F. Fohlmeister and R. F. Miller, "Impulse encoding mechanisms of ganglion cells in the tiger salamander retina," *J Neurophysiol,* vol. 78, pp. 1935-1947, 1997.

[11] J. D. Engbers, D. Anderson, R. Tadayonnejad, W. H. Mehaffey, M. L. Molineux, and R. W. Turner, "Distinct roles for I(T) and I(H) in controlling the frequency and timing of rebound spike responses," *J Physiol,* vol. 589, pp. 5391-5413, 2011.

[12] A. L. Hodgkin and A. F. Huxley, "A quantitative description of membrane current and its application to conduction and excitation in nerve," *J Physiol,* vol. 117, pp. 500-544, 1952.

[13] M. L. Hines and N. T. Carnevale, "The NEURON simulation environment," *Neural Computation,* vol. 9, pp. 1179-1209, 1997.

[14] T. Guo, D. Tsai, J. W. Morley, G. J. Suaning, N. H. Lovell, and S. Dokos, "Influence of Cell Morphology in a Computational Model of ON and OFF Retinal Ganglion Cells," in *Engineering in Medicine and Biology Society (EMBC), 2013 Annual International Conference of the IEEE*, accepted.

[15] S. Dokos and N. H. Lovell, "Parameter estimation in cardiac ionic models," *Prog Biophys Mol Biol,* vol. 85, pp. 407-431, 2004.

[16] R. F. Miller, K. Stenback, D. Henderson, and M. Sikora, "How voltage-gated ion channels alter the functional properties of ganglion and amacrine cell dendrites," *Arch Ital Biol,* vol. 140, pp. 347-359, 2002.